coatings

MDPI

Article

Phase Composition and Stability, Sintering and Thermal Conductivity of Gd_2O_3 and Yb_2O_3 Co-Doped YSZ

He Tian [1,2], Liangliang Wei [1,*] and Limin He [2]

[1] School of Materials Science and Engineering, Beihang University, No. 37 Xueyuan Road, Beijing 100191, China
[2] Key Laboratory of Advanced Corrosion and Protection for Aviation Materials, Beijing Institute of Aeronautical Materials, Aero Engine Corporation of China, Beijing 100095, China
* Correspondence: weill@buaa.edu.cn

Abstract: Y_2O_3-stabilized ZrO_2 (YSZ) has been the material of choice for thermal barrier coatings (TBCs) in the past decades, yet its phase decomposition limits its application above 1200 °C. In this study, Gd_2O_3 and Yb_2O_3 co-doped YSZ powders were produced, in which some amounts of monoclinic (m) phase were introduced into the cubic (c) phase matrix. XRD results showed that the fabricated powders obtained by a solid phase synthesis were composed of m and c phases, and hat the m phase content decreased in a sequence of 4Gd-2Yb-4Y, 2Gd-2Yb-6Y and 2Gd-4Yb-4Y powders. This indicated that Yb^{3+} is an excellent stabilizer in the ZrO_2-based lattice, which could largely suppress the formation of the m phase. The m phase content in the powders was almost kept unchanged with heating at 1300 °C, which could provide a toughening effect to the ceramic. All the powders exhibited no obvious sintering at 1300 °C for 150 h. As compared to YSZ, the three fabricated ceramics had lower thermal conductivities, and they increased in a sequence of 4Gd-2Yb-4Y, 2Gd-4Yb-4Y and 2Gd-2Yb-6Y.

Keywords: thermal barrier coatings; YSZ; co-doping; phase stability; thermal conductivity

check for updates

Citation: Tian, H.; Wei, L.; He, L. Phase Composition and Stability, Sintering and Thermal Conductivity of Gd_2O_3 and Yb_2O_3 Co-Doped YSZ. *Coatings* **2023**, *13*, 53. https://doi.org/10.3390/coatings13010053

Academic Editor: Salvatore Grasso

Received: 14 November 2022
Revised: 7 December 2022
Accepted: 8 December 2022
Published: 28 December 2022

1. Introduction

ZrO_2 stabilized by oxides has been extensively studied, and one of the representative stabilizers is Y_2O_3 [1–3]. Due to its excellent high-temperature mechanical and thermal–physical properties, Y_2O_3 partially stabilized ZrO_2 (YSZ) has been practically applied in electronics [4,5], atomic energy, the aviation industry, and especially to the thermal barrier coatings (TBC) which offer thermal insulation to the hot components of aero-engines and thus effectively improve their combustion efficiency [6–8]. YSZ TBCs have been successfully used for several decades [9,10], but they have become less and less reliable with the development of aero-engines [11–14]. One crucial aspect in this is issue of the phase decomposition and phase transformation [1,15,16]. As is known to all, YSZ TBCs are usually prepared either by electron beam physical vapor deposition (EB-PVD) [17,18] or by air plasma spraying (APS) [19–21]. Additionally, they exhibit a non-transformable metastable tetragonal (t') phase, which is desirable for thermal insulation yet. At temperatures above 1200 °C [22], the t'-YSZ decomposes into cubic (c)-YSZ and t YSZ, the latter transforming into a monoclinic (m) phase accompanied by some volume expansion [23,24], which is fast and uncontrollable [25]. When the phase-transformed part reaches a critical value, the resulting volume expansions lead to crack initiation, propagation, and even coating spallation.

Many efforts have been made to enhance the high-temperature phase instability of the t'-YSZ, such as selecting alternate stabilizers to Y_2O_3 for ZrO_2-based systems. Cairney et al. reported that the phase stability of ZrO_2, stabilized by Yb_2O_3, is better than that of YSZ at 1300 °C [26]. Er_2O_3, Sm_2O_3, Nd_2O_3, Sc_2O_3 and Gd_2O_3 have also been studied as stabilizers for ZrO_2, and Er_2O_3-ZrO_2 has the best phase stability [27–32]. It is worthy

noted that the Gd_2O_3 dopant improves the sintering resistance of both bulk Gd_2O_3-ZrO_2 (4 mol% stabilizer) and YSZ TBCs, although it decreases the t′ phase stability, as reported by Rahaman [27]. Er_2O_3, Sm_2O_3, and Nd_2O_3 have also been studied as stabilizers for ZrO_2, and the t′ phase stability of Er_2O_3-ZrO_2 is the best [28]. Additionally, some reports have revealed that co-doping two or more rare earth oxides (RE_2O_3) into ZrO_2 has an effective function in improving the t′ phase stability. Guo et al. found better t′ phase stability in Sc_2O_3-Gd_2O_3-ZrO_2 ceramics with increasing Sc_2O_3 content [33]. Moreover, Guo et al. has analyzed the t′ phase stability of RE_2O_3 (RE = La, Nd, Gd, Yb)-Yb_2O_3-YSZ at 1400 °C [34].

Although the modified t′ phase stability has improved at high temperatures, it still inevitably undergoes phase decomposition with long-term annealing. Despite its excellent thermal conductivity and high-temperature phase stability, C-ZrO_2 is unfortunately not tough enough for use in TBCs because of its low toughness [15]. The volume expansion, resulting from the t to m phases transformation, can absorb or consume the energy at the crack tip and generate compressive stresses in the region of the main crack action, something which improves the strength and fracture toughness of the coating [20]. Therefore, it is reasonable to believe that setting an appropriate amount of m phase in the c-ZrO_2 and maintaining the m phase content during service can effectively improve the performance of ZrO_2 ceramics.

In this study, we prepared YSZ co-doped with Gd_2O_3 and Yb_2O_3 via a solid-state reaction, which consisted of c and m phases. An investigation was conducted into the effect of co-doped RE_2O_3 on the monoclinic. The phase stability of the fabricated powders which were heat-treated at 1300 °C was evaluated. In addition, the sintering behavior and thermal conductivity of the co-doped ZrO_2 ceramics were investigated and compared with those of YSZ. Finally, the mechanisms of the reduced thermal conductivity, resulting from the rare earth co-doping, were discussed.

2. Experimental Procedure

The co-doped ZrO_2 were prepared by solid-state reaction at 1400 °C for 12 h, using Gd_2O_3, Yb_2O_3, Y_2O_3 (99.99% purity) and ZrO_2 (99.9% purity) as raw materials. The total stabilizer content of each doped zirconia is 10 mol%, and the specific components are expressed in mol% as follows: $2Gd_2O_3$-$2Yb_2O_3$-$6Y_2O_3$-$90ZrO_2$ (2Gd-2Yb-6Y), $2Gd_2O_3$-Yb_2O_3-Y_2O_3-$90ZrO_2$ (2Gd-4Yb-4Y), and $4Gd_2O_3$-$2Yb_2O_3$-$4Y_2O_3$-$90ZrO_2$ (4Gd-2Yb-4Y). The raw powers were mixed in a planetary ball mill with absolute ethanol for more than 12 h to obtain a homogeneous mixture. The homogeneously mixed solution was dried, placed in a zirconia crucible at 1400 °C and sintered for 12 h to produce RE_2O_3-stabilized ZrO_2 ceramics. Meanwhile, some mixed powder was cold-pressed at 250 MPa and then sintered at 1400 °C for 10 h to obtain the bulk material for thermal conductivity measurements. A scanning electron microscope (SEM; JEOL 7900F) was used to characterize the morphologies of ceramic powders after calcination and annealing at 1300 °C for 50h, 100, and 150 h. Phase stability was characterized by X-ray diffraction (X'Pert^3 MRD, Malvern Panalytical, Cu Kα radiation). The scanning frequency was 0.05°/s. The molar content of the m phase was calculated using Miller's formula [35], given in Equations (1) and (2):

$$\frac{M_m}{M_{c,t}} = 0.82\frac{I_m(\bar{1}11)+I_m(111)}{I_{c,t}(111)} \quad (1)$$

$$M_m + M_{c,t} = 1 \quad (2)$$

where M_m and $M_{c,t}$ are the mole fractions of the m and c/t phases, respectively, and I is the integrated intensity corresponding to the peaks concerned.

The thermal diffusivity (α) of RE_2O_3 co-doped ZrO_2 was measured between 20 °C and 1200 °C using a laser flash meter (LFA 427; Netzsch, Selb, Germany), with an interval temperature of 200 °C. Before measuring the thermal diffusivity, the front and back surface of the samples were coated with a graphite film to allow thermal absorption of the laser pulse. Each sample was measured three times at selected temperatures. The specific heat

capacity (C_p) is calculated from the heat capacity values of the individual constituent oxide based on the Neumann-Kopp rule [36]. The density (ρ) was measured by the Archimedes' method. The thermal conductivity (λ) was calculated by Equation (3):

$$\lambda = \rho \cdot \alpha \cdot C_p \tag{3}$$

Since the sintered sample cannot be completely dense, the influence (ϕ) on the thermal conductivity of the material can be fixed using the following equation, in which λ_0 expresses the full density of the sample (λ_0) [37]:

$$\frac{\lambda}{\lambda_0} = 1 - \frac{4}{3}\phi \tag{4}$$

3. Results and Discussion

Figure 1 shows the XRD patterns of the as-fabricated 2Gd-2Yb-6Y, 4Gd-2Yb-4Y and 2Gd-4Yb-4Y powders. For all samples, the primary phase is the c phase. In the range between $2\theta \approx 28.3^\circ$ and 31.5° of all the patterns the diffraction peaks were found, which are characteristic peaks of the m phase. Hence, it could be identified that the fabricated powders are composed of c and m phases. The m phase contents in the three types of co-doped ZrO_2 were calculated and illustrated in Figure 2. It could be found that the m phase content in the samples increases in a sequence of 2Gd-4Yb-4Y, 2Gd-2Yb-6Y and 4Gd-2Yb-4Y powders.

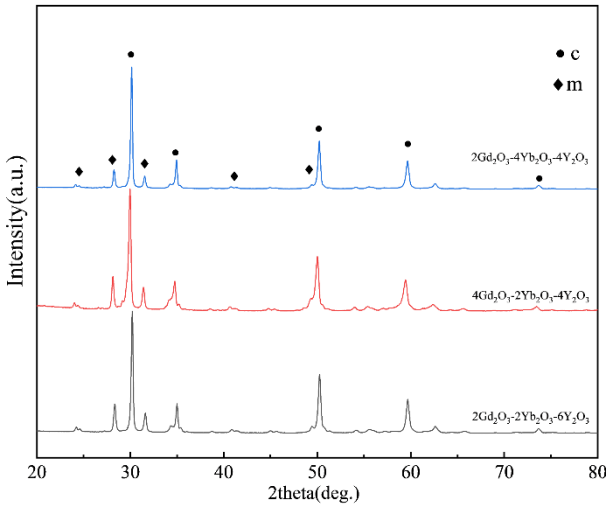

Figure 1. XRD patterns of as-fabricated 2Gd-2Yb-6Y, 4Gd-2Yb-4Y and 2Gd-4Yb-4Y powders.

The different m contents in the three samples could be attributed to the difference in the stabilization ability of Yb, Y and Gd. When rare earth cations are used to stabilize ZrO_2, a smaller size misfit between RE^{3+} and Zr^{4+} ions in the ZrO_2 lattice is desirable. The cation radii of Yb^{3+}, Y^{3+}, Gd^{3+} and Zr^{4+} are 0.985 Å, 1.019 Å, 1.053 Å and 0.84 Å in the 8-coordination, respectively. Thus, doping Yb^{3+} into the ZrO_2 lattice is considered to have the most ability to obtain a stable c phase [38]. Based on this consideration, the variation tendency of the m phase content in the samples could be well explained. Comparing samples 2Gd-4Yb-4Y and 2Gd-2Yb-6Y, they have the same range of Gd, but the first sample is rich in Yb, while the second is rich in Y. Since Yb^{3+} is smaller than Y^{3+}, it is reasonable that the 2Gd-4Yb-4Y sample has a higher content of c phase content than the 2Gd-2Yb-6Y sample. Thus, the content of m phase in the 2Gd-4Yb-4Y sample is lower than that in the 2Gd-2Yb-6Y sample. The Yb contents of the 2Gd-2Yb-6Y and 4Gd-2Yb-4Y samples are identical, but the former contains lower Y^{3+} levels. Hence, the 2Gd-2Yb-6Y sample has a higher ability to produce the c phase, and its m phase content is lower. Therefore, the m phase content follows the sequence $m_{2Gd\text{-}4Yb\text{-}4Y} < m_{2Gd\text{-}2Yb\text{-}6Y} < m_{4Gd\text{-}2Yb\text{-}4Y}$, further

evidence that Yb^{3+} is an excellent stabilizer in the ZrO_2 lattice that can largely suppress the formation of the m phase.

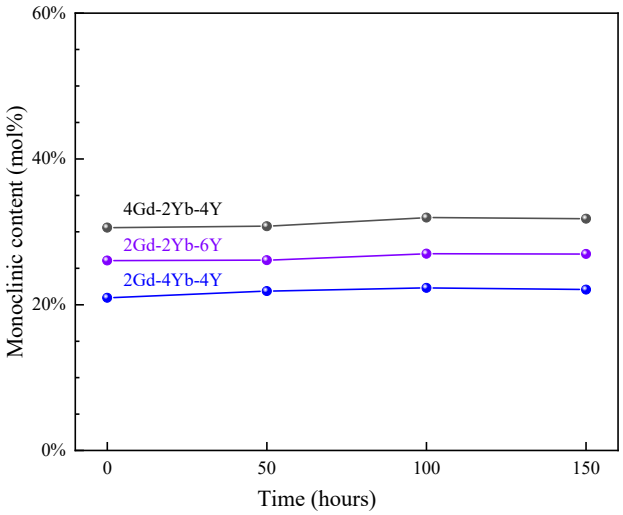

Figure 2. M phase contents of 2Gd-2Yb-6Y, 4Gd-2Yb-4Y and 2Gd-4Yb-4Y powders with time at 1300 °C.

The lattice parameters of the c phase in the powders 2Gd-2Yb-6Y, 4Gd-2Yb-4Y and 2Gd-4Yb-4Y were calculated, and the results are listed in Table 1. It was found that the lattice parameters of the samples increase in a sequence of 2Gd-4Yb-4Y, 2Gd-2Yb-6Y and 4Gd-2Yb-4Y. This could also be explained based upon the difference in the RE^{3+} radius. By comparing 2Gd-2Yb-6Y and 4Gd-2Yb-4Y, their Yb contents are identical, but the latter contains more Gd^{3+}. Thus, 4Gd-2Yb-4Y has a more significant lattice parameter than 2Gd-2Yb-6Y. For the case of 2Gd-2Yb-6Y and 4Gd-2Yb-4Y, the Yb contents are the same, but 2Gd-2Yb-6Y contains more Y and thus shows a smaller lattice parameter.

Table 1. Lattice parameters in different ceramic samples.

Gd_2O_3 mol%	Yb_2O_3 mol%	Y_2O_3 mol%	a = b = c (Å)
		10	5.138
2	2	6	5.133
4	2	4	5.151
2	4	4	5.131

To investigate the changes in the phase structure of the co-doped zirconia powder at 1300 °C, heat treatment tests were performed at different times. Figure 3 shows the XRD patterns of 2Gd-2Yb-6Y, 4Gd-2Yb-4Y and 2Gd-4Yb-4Y powders at different heat treatment times. The c and m phases are still present at each time point, and the changes in m phase content in the samples are shown in Figure 2. It can be seen that the m phase contents in all samples remain almost unchanged with the heating time. 2Gd-2Yb-6Y, 4Gd-2Yb-4Y and 2Gd-4Yb-4Y are composed of c and m phases. It is known that the c phase does not undergo any transformation during heat treatments. Therefore, it is reasonable to keep the content of m phase constant after heat treatment. However, the m phase undergoes transformation during heat treatment. It transforms into a t phase, and the t→m phase transition occurs during the subsequent cooling process. This process belongs to the martensitic transformation, a phenomenon which can provide a toughening effect to the ceramic. As a result, 2Gd-2Yb-6Y, 4Gd-2Yb-4Y and 2Gd-4Yb-4Y are expected to have higher toughness than those with a pure c phase. Even though, it should be noted that the proportion of m phase in the sample should not be too high as this would be detrimental to the ceramics for TBC applications [39,40].

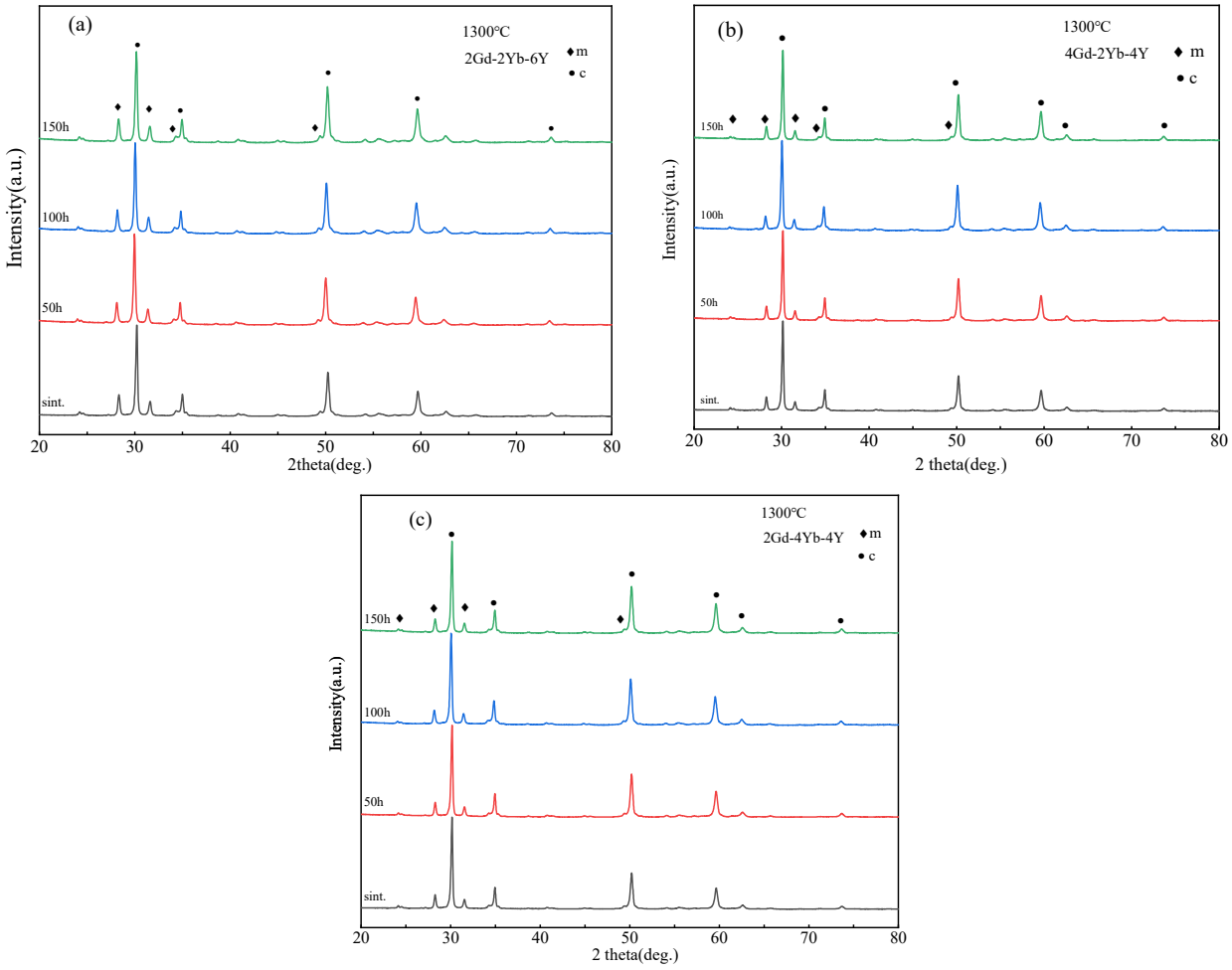

Figure 3. XRD patterns of (**a**) 2Gd-2Yb-6Y, (**b**) 4Gd-2Yb-4Y and (**c**) 2Gd-4Yb-4Y powders after 50, 100 h and 150 h at 1300 °C.

Figure 4 shows the microstructure of the powders after 150 h of heat treatment. All samples showed good sintering resistance, with most powders maintaining an independent grain shape. In the 2Gd-2Yb-6Y powder, many separated grains were connected by a neck structure, the neck between the grains grew significantly, the deformation of the grains was more significant, and a clear trend of grain boundary movement was found. Conversely, in the 4Gd-2Yb-4Y and 2Gd-4Yb-4Y powders, most of the grains still maintained an independent polygonal structure with fewer and smaller necks, indicating a lower degree of sintering in these two ceramic samples. The microscopic mechanism of the initial sintering of ceramic powders is the lattice diffusion from the inner grain boundary to the neck. The low sintering rate of polyoxides-doped ZrO_2 is reasonable, Gd^{3+} has a large ionic radius, and its distribution requires higher energy. In contrast, Yb^{3+} has a smaller ionic radius, but its larger atomic mass also limits the grain boundary diffusion, a factor which improves the sintering resistance of ceramics. This is consistent with the cation distribution in Figure 5 over 150 h. Therefore, the degree of sintering is also lower. Since the ceramic samples in this study are a mixture of c and m phases, which increases the energy required for grain boundary movement, and thus doping with Gd_2O_3, Yb_2O_3, and, Y_2O_3 helps to improve the resistance of the ZrO_2-based ceramics.

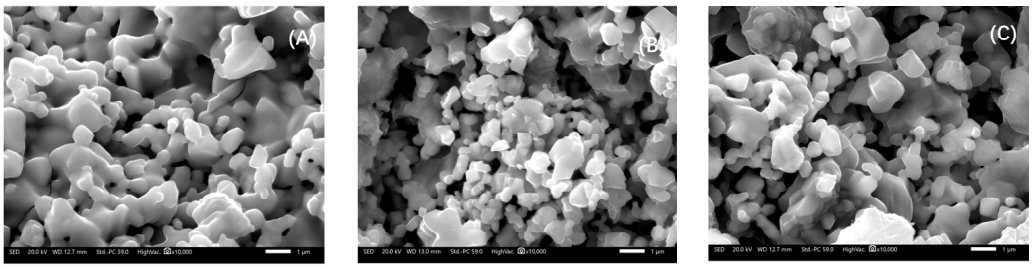

(**a**) 2Gd-2Yb-6Y (**b**) 4Gd-2Yb-4Y (**c**) 2Gd-4Yb-4Y

Figure 4. Microstructure of different component powders after 150 h at 1300 °C.

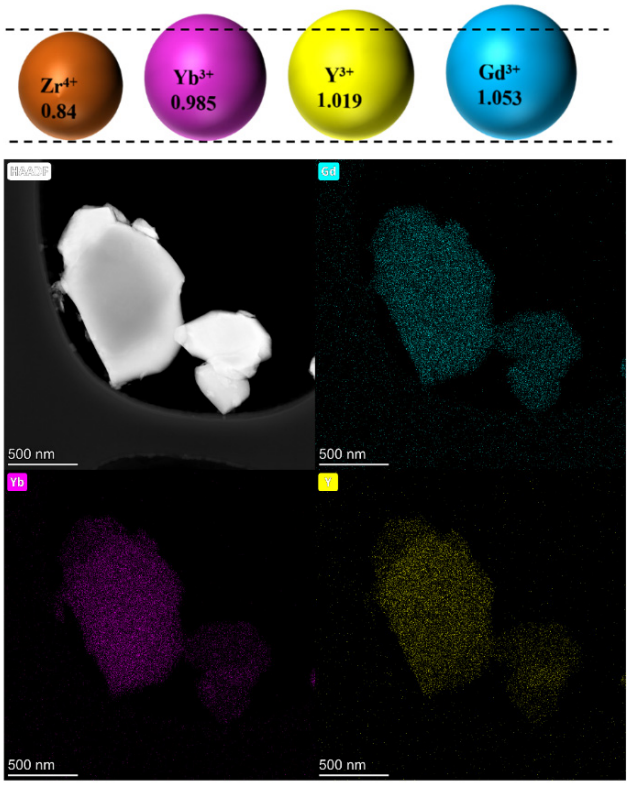

Figure 5. Elemental distribution of the 2Gd-4Yb-4Y powder after heat treatment for 150 h at 1300 °C.

Figure 6 shows the thermal conductivities of 2Gd-2Yb-6Y, 4Gd-2Yb-4Y, 2Gd-4Yb-4Y and YSZ ceramics. The error bars are neglected because they are smaller than the symbols. Firstly, the thermal conductivity of ceramics decreases with increasing temperature in the room temperature range up to 800–1000 °C and increases when the temperature exceeds 1000 °C. Secondly, it is found that all the co-doped ceramics have lower thermal conductivities than YSZ. At 1000 °C, the thermal conductivities of 2Gd-2Yb-6Y, 2Gd-4Yb-4Y, and 4Gd-2Yb-4Y are 1.889 W/mK, 1.663 W/mK and 1.420 W/mK, respectively.

It is well known that thermal conductivity is highly dependent on the non-harmonic effects caused by phonon scattering and on the vacancies caused by defects [41,42]. In this study, co-doping with RE_2O_3 causes more defects and elastic strain fields, reducing phonons average free range and leading to the lower thermal conductivity of ZrO_2 co-doped with Gd_2O_3, Yb_2O_3, and Y_2O_3 than YSZ.

For the ZrO_2 doped with RE_2O_3, the phonon scattering rates can be expressed with the following Equation (5) [43] due to the different atomic masses of doped RE^{3+} and Zr^{4+}:

$$\frac{1}{\tau_{\Delta M}(\omega)} = \frac{ca^3\omega^4}{4\pi {v_s}^3}\left(\frac{\Delta M}{M}\right)^2 \quad (5)$$

where τ is the relaxation time, α^3 is the atomic volume, v_s is the transverse wave velocity, ω is the phonon frequency, c is the ratio of the number of defects per unit volume focus to the number of dot positions, M is the Zr^{4+} mass of cation, and ΔM is the mass difference between the doped RE^{3+} and Zr^{4+}. The scattering rate of the phonons is proportional to the square of ΔM. Thus, the larger the mass difference between the doped cations and Zr^{4+} is, the stronger the phonon scattering will be, resulting in lower thermal conductivity. Therefore, ceramics prepared in this study have lower thermal conductivities.

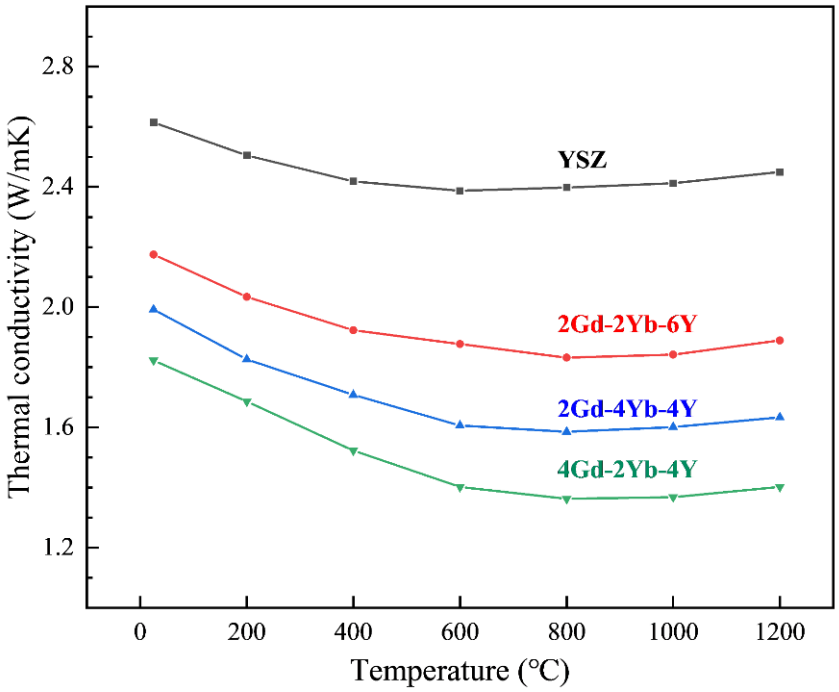

Figure 6. The thermal conductivity of the specimens as a function of temperature.

The doping of RE_2O_3 to YSZ produces an elastic field due to the difference in ionic radii between RE^{3+} and Zr^{4+}, dislodging surrounding atoms and altering the phonon frequency.

Due to the difference in ionic radius between RE^{3+} and Zr^{4+}, doping YSZ with RE_2O_3 produces an elastic field, which dislodges atoms and affects phonon frequencies, enhancing phonon scattering [43]:

$$\frac{1}{\tau_{\Delta R}(\omega)} = \frac{2ca^3\omega^4}{\pi v^3} J^2\gamma^2\left(\frac{\Delta R}{R}\right)^2 \quad (6)$$

where J is a constant, γ is the Gruneisen's constant, R is the Zr^{4+} cation radius, and ΔR is the radius difference between the doped RE^{3+} and Zr^{4+}. Thus, the larger the radius difference between the doped cations and Zr^{4+}, the stronger the phonon scattering, resulting in lower thermal conductivity. Hence, the fabricated ceramics in this study are shown to have lower thermal conductivities compared to YSZ.

As shown in Figure 6, the thermal conductivities of the co-doped samples increase in an order of 4Gd-2Yb-4Y, 2Gd-4Yb-4Y and 2Gd-2Yb-6Y, which could be explained by the basis of the above discussion on the effects of ΔM and ΔR on the phonon scattering. In comparison, the Y2O3 content of 4Gd-2Yb-4Y and 2Gd-4Yb-4Y ceramics is the same. Thus, only the impact of Gd and Yb on the phonon scattering needs to be considered. Compared to Yb^{3+}, Gd^{3+} is larger and lighter. Thus ΔR (Gd^{3+}-Zr^{4+}) is larger than ΔR (Yb^{3+}-Zr^{4+}), but ΔM (Gd^{3+}-Zr^{4+}) is smaller than ΔM (Yb^{3+}-Zr^{4+}). Since 4Gd-2Yb-4Y has lower thermal conductivities than 2Gd-4Yb-4Y, it could be implied that the ΔR plays a more dominant role in affecting phonon scattering than the ΔM for those two ceramics. For the 2Gd-4Yb-4Y and 2Gd-2Yb-6Y ceramics, ΔM (Yb^{3+}-Zr^{4+}) is larger than ΔM (Y^{3+}-Zr^{4+}), but ΔR (Yb^{3+}-Zr^{4+}) is smaller than ΔR (Y^{3+}-Zr^{4+}). 2Gd-4Yb-4Y has lower thermal conductivities than 2Gd-2Yb-6Y,

which implies that in this case, the ΔM plays a more dominant role in affecting the phonon scattering than the ΔR.

4. Conclusions

10 mol% for Gd_2O_3, Yb_2O_3, and Y_2O_3 co-doped ZrO_2 was synthesized by the solid-state reaction method:

1. Analysis of the phase content analysis of the synthesized powders revealed that the content of m phase gradually decreased for the powders 4Gd-2Yb-4Y, 2Gd-2Yb-6Y, and 2Gd-4Yb-4Y. This suggests that Yb_2O_3 effectively suppresses the formation of the m phase and is an excellent stabilizer for ZrO_2. A subsequent heat treatment test at 1300 °C, conducted for 150 h, showed that m phase remained almost unchanged, indicating that it can significantly improve the toughness of a given material.
2. No sintering was observed in any of the powders, suggesting that the addition of Gd_2O_3 and Yb_2O_3 improves the sintering resistance of YSZ materials.
3. Co-doping Gd_2O_3 and Yb_2O_3 can effectively reduce the thermal conductivity of YSZ. The co-doping increases the discrepancy between the radius and atomic mass of RE^{3+} and Zr^{4+} ions, which increases the phonon scattering and reduces the thermal conductivity of the material, resulting in increased phonon scattering. The experimental results indicate the Gd_2O_3 is more effective at decreasing thermal conductivity than co-doped ZrO_2.

As a result of these comprehensive properties, 4Gd-2Yb-4Y ceramics may be considered a promising candidate for TBC manufacturing. Additionally, more work will focus on the mechanical properties of 4Gd-2Yb-4Y materials and the performance of coatings with this composition.

Author Contributions: Writing—original draft preparation, data curation, formal analysis, and investigation, H.T.; review and editing, L.W.; funding acquisition, L.W. and L.H. All authors have read and agreed to the published version of the manuscript.

Funding: This research was funded for National Natural Science Foundation of China in 2021, design and functional realization mechanism of high temperature ablation resistant, highly efficient thermal insulation and large strain tolerance protective coatings.

Institutional Review Board Statement: Not applicable.

Informed Consent Statement: Not applicable.

Data Availability Statement: Data is contained within the article.

Conflicts of Interest: The authors declare no conflict of interest.

References

1. Padture, N.P. Advanced structural ceramics in aerospace propulsion. *Nat. Mater.* **2016**, *15*, 804–809. [CrossRef] [PubMed]
2. Clarke, D.R.; Levi, C.G. Materials Design for the Next Generation Thermal Barrier Coatings. *Annu. Rev. Mater. Res.* **2003**, *33*, 383–417. [CrossRef]
3. Clarke, D.R.; Oechsner, M.; Padture, N.P. Thermal-barrier coatings for more efficient gas-turbine engines. *MRS Bull.* **2012**, *37*, 891–898. [CrossRef]
4. Nomura, M.; Kage, Y.; Müller, D. Electrical and thermal properties of polycrystalline Si thin films with phononic crystal nanopatterning for thermoelectric applications. *Appl. Phys. Lett.* **2015**, *106*, 223106. [CrossRef]
5. Yanagisawa, R.; Tsujii, N.; Mori, T. Nanostructured planar-type uni-leg Si thermoelectric generators. *Appl. Phys. Express* **2020**, *13*, 095001. [CrossRef]
6. Clarke, D.R.; Phillpot, S.R. Thermal barrier coating materials. *Mater. Today* **2005**, *8*, 22–29. [CrossRef]
7. Vassen, R.; Cao, X.Q.; Tietz, F. Zirconates as new materials for thermal barrier coatings. *J. Am. Ceram. Soc.* **2000**, *83*, 2023–2028. [CrossRef]
8. Sun, C.; Hui, R.; Roller, J. Cathode materials for solid oxide fuel cells: A review. *J. Solid State Electrochem.* **2010**, *14*, 1125–1144. [CrossRef]
9. Kakuda, T.R.; Limarga, A.M. Evolution of thermal properties of EB-PVD 7YSZ thermal barrier coatings with thermal cycling. *Acta Mater.* **2009**, *57*, 2583–2591. [CrossRef]

10. Evans, A.G.; Clarke, D.R. The influence of oxides on the performance of advanced gas turbines. *J. Eur. Ceram. Soc.* **2008**, *28*, 1405–1419. [CrossRef]
11. Darolia, R. Thermal barrier coatings technology: Critical review, progress update, remaining challenges and prospects. *Int. Mater. Rev.* **2013**, *58*, 315–348. [CrossRef]
12. Wang, Y.; Zhou, C. Hot corrosion behavior of nanostructured Gd_2O_3 doped YSZ thermal barrier coating in presence of Na_2SO_4 + V_2O_5 molten salts. *Prog. Nat. Sci. Mater. Int.* **2017**, *27*, 507–513. [CrossRef]
13. Wang, C.; Zinkevich, M.; Aldinger, F. Phase diagrams and thermodynamics of rare-earth-doped zirconia ceramics. *Pure Appl. Chem.* **2007**, *79*, 1731–1753. [CrossRef]
14. Lu, X.; Xu, P.; Wang, H. Cooling potential and applications prospects of passive radiative cooling in buildings: The current state-of-the-art. *Renew. Sustain. Energy Rev.* **2016**, *65*, 1079–1097. [CrossRef]
15. Vasanthavel, S.; Kannan, S. Structural investigations on the tetragonal to cubic phase transformations in zirconia induced by progressive yttrium additions. *J. Phys. Chem. Solids* **2018**, *112*, 100–105. [CrossRef]
16. Hurwitz, F.I.; Rogers, R.B.; Guo, H. Phase development and pore stability of yttria- and ytterbia-stabilized zirconia aerogels. *J. Am. Ceram. Soc.* **2020**, *103*, 6700–6711. [CrossRef]
17. Ochrombel, R.; Schneider, J.; Hildmann, B. Thermal expansion of EB-PVD yttria stabilized zirconia. *J. Eur. Ceram. Soc.* **2010**, *30*, 2491–2496. [CrossRef]
18. Naraparaju, R.; Hüttermann, M.; Schulz, U. Tailoring the EB-PVD columnar microstructure to mitigate the infiltration of CMAS in 7YSZ thermal barrier coatings. *J. Eur. Ceram. Soc.* **2017**, *37*, 261–270. [CrossRef]
19. Lashmi, P.G.; Ananthapadmanabhan, P.V.; Unnikrishnan, G. Present status and future prospects of plasma sprayed multilayered thermal barrier coating systems. *J. Eur. Ceram. Soc.* **2020**, *40*, 2731–2745. [CrossRef]
20. Ponnuchamy, M.B.; Gandhi, A.S. Phase and fracture toughness evolution during isothermal annealing of spark plasma sintered zirconia co-doped with Yb, Gd and Nd oxides. *J. Eur. Ceram. Soc.* **2015**, *35*, 1879–1887. [CrossRef]
21. Lima, R.S. Perspectives on Thermal Gradients in Porous ZrO_2-7~8 wt.% Y_2O_3 (YSZ) Thermal Barrier Coatings (TBCs) Manufactured by Air Plasma Spray (APS). *Coatings* **2020**, *10*, 812. [CrossRef]
22. Clarke, D.R.; Levi, C.G. Enhanced zirconia thermal barrier coating systems. *Proc. Inst. Mech. Eng. Part A J. Power Energy* **2006**, *220*, 85–92. [CrossRef]
23. Ren, X.; Pan, W. Mechanical properties of high-temperature-degraded yttria-stabilized zirconia. *Acta Mater.* **2014**, *69*, 397–406. [CrossRef]
24. Fu, Z.; Wu, N.; Long, H. Fabrication of Highly Transparent Y_2O_3 Ceramics via Colloidal Processing Using ZrO_2-Coated Y_2O_3 Nanoparticles. *Coatings* **2022**, *12*, 1077. [CrossRef]
25. Guo, L.; Zhang, C.; Xu, L. Effects of TiO_2 doping on the defect chemistry and thermo-physical properties of Yb_2O_3 stabilized ZrO_2. *J. Eur. Ceram. Soc.* **2017**, *37*, 4163–4169. [CrossRef]
26. Cairney, J.M.; Rebollo, N.R.; Rühle, M. Phase stability of thermal barrier oxides: A comparative study of Y and Yb additions. *Int. J. Mater. Res.* **2007**, *98*, 1177–1187. [CrossRef]
27. Rahaman, M.; Gross, J.; Dutton, R. Phase stability, sintering, and thermal conductivity of plasma-sprayed ZrO_2–Gd_2O_3 compositions for potential thermal barrier coating applications. *Acta Mater.* **2006**, *54*, 1615–1621. [CrossRef]
28. Boissonnet, G.; Chalk, C.; Nicholls, J.R. Phase stability and thermal insulation of YSZ and erbia-yttria co-doped zirconia EB-PVD thermal barrier coating systems. *Surf. Coat. Technol.* **2020**, *389*, 125566. [CrossRef]
29. Jones, R.L.; Mess, D. Improved tetragonal phase stability at 1400 °C with scandia, yttria-stabilized zirconia. *Surf. Coat. Technol.* **1996**, *86*, 94–101. [CrossRef]
30. Leoni, M.; Jones, R.L.; Scardi, P. Phase stability of scandia–yttria-stabilized zirconia TBCs. *Surf. Coat. Technol.* **1998**, *108*, 107–113. [CrossRef]
31. Fan, W.; Wang, Y.; Liu, Y. Mechanical Properties Durability of Sc_2O_3-Y_2O_3 Co-Stabilized ZrO_2 Thermal Barrier Materials for High Temperature Application. *Coatings* **2022**, *12*, 155. [CrossRef]
32. Yan, Z.; Peng, H.; Yuan, K. Optimization of Yb_2O_3-Gd_2O_3-Y_2O_3 Co-Doped ZrO_2 Agglomerated and Calcined Powders for Air Plasma Spraying. *Coatings* **2021**, *11*, 373. [CrossRef]
33. Sun, L. Influence of partial substitution of Sc_2O_3 with Gd_2O_3 on the phase stability and thermal conductivity of Sc_2O_3-doped ZrO_2. *Ceram. Int.* **2013**, *39*, 3447–3451. [CrossRef]
34. Guo, L.; Li, M.; Ye, F. Phase stability and thermal conductivity of RE_2O_3 (RE = La, Nd, Gd, Yb) and Yb_2O_3 co-doped Y_2O_3 stabilized ZrO_2 ceramics. *Ceram. Int.* **2016**, *42*, 7360–7365. [CrossRef]
35. Miller, R.A. Phase stability in plasma sprayed partially stabilized zirconia-yttria. *Am. Ceram. Soc.* **1981**, *3*, 241–253.
36. Kubaschewski, O. *Materials Thermochemistry*, 6th ed.; Pergamon Press: Oxford, UK, 1993; pp. 254–326.
37. Wu, J.; Wei, X.Z.; Padture, N.P. Low-thermal-conductivity rare-earth zirconates for potential thermal-barrier-coating applications. *J. Am. Ceram. Soc.* **2002**, *85*, 3031–3035. [CrossRef]
38. Zacate, M.O.; Minervini, L. Defect cluster formation in M_2O_3-doped cubic ZrO_2. *Solid State Ion.* **2000**, *128*, 243–254. [CrossRef]
39. Xue, M.; Liu, S.; Wang, X. High fracture toughness of 3Y-TZP ceramic over a wide sintering range. *Mater. Chem. Phys.* **2020**, *244*, 122693. [CrossRef]
40. Zhang, Y.; Guo, L.; Zhao, X. Toughening effect of Yb_2O_3 stabilized ZrO_2 doped in $Gd_2Zr_2O_7$ ceramic for thermal barrier coatings. *Mater. Sci. Eng. A* **2015**, *648*, 385–391. [CrossRef]

41. Tian, Z.; Lin, C.; Zheng, L. Defect-mediated multiple-enhancement of phonon scattering and decrement of thermal conductivity in $(Y_xYb_{1-x})_2SiO_5$ solid solution. *Acta Mater.* **2018**, *144*, 292–304. [CrossRef]
42. Ishibe, T.; Tomeda, A.; Komatsubara, Y. Carrier and phonon transport control by domain engineering for high-performance transparent thin film thermoelectric generator. *Appl. Phys. Lett.* **2021**, *118*, 151601. [CrossRef]
43. Berman, R. *Thermal Conduction in Solid*; Clarendon Press: Oxford, UK, 1976.